Available online at www.sciencedirect.com

SciVerse ScienceDirect

Procedia Engineering 00 (2012) 000–000

Procedia Engineering

www.elsevier.com/locate/procedia

5th BSME International Conference on Thermal Engineering

Stability theory and experiments in wall-turbulence

P.K. Sen*, S. V. Veeravalli and Ganapati Joshi#

Indian Institute of Technology Delhi, New Delhi - 110016, India

Abstract

Drag reduction is one of the most important areas of research. The main concept behind drag reduction is turbulence control. This could possibly be achieved in near wall turbulent flow by suppressing wall-mode instabilities (i.e., by interfering with the seeding mechanism of turbulence production). Wall-mode instabilities can be studied by applying hydrodynamic stability theory to wall bounded turbulent flows. It has been shown in Sen & Veeravalli, 2000 (*Sadhana*, 25, 423-437) that an anisotropic eddy viscosity model is crucial in capturing the wall mode instabilities. The main results of this theory are discussed and we present detailed experimental investigations carried out with the objective of verifying the Sen & Veeravalli theory.

Keywords: *Stability theory; wall-turbulence; T-S waves; eddy viscosity; turbulence control.*

Nomenclature

H	Channel half width	u	Velocity fluctuation
U	Instantaneous velocity	$\tilde{u}$	Velocity component due to organised disturbance
$\overline{U}$	Mean velocity		
U_o	Centreline velocity	f	Frequency of organised wave
V	Sectional average velocity	α	Wave number, complex
$\mathrm{Re} \equiv \frac{U_o H}{\nu}$	Reynolds Number (using U_o)	α_r	Wave number, real
		α_i	Wave number, imaginary
$R \equiv \frac{VH}{\nu}$	Reynolds Number (using V)	$\beta = 2\pi f$	Circular frequency
		k	Turbulent kinetic energy
c	Wave speed, complex	ε	Eddy viscosity
c_r	Wave speed, real	ε_d	Turbulent dissipation rate
c_i	Wave speed, imaginary	θ	Phase angle
c_g	Group velocity	ψ	Stream function
P	Instantaneous pressure	ϕ	Eigenfunction
p	Pressure fluctuation	λ	Anisotropy function
$\tilde{p}$	Pressure component due to organised disturbance	κ	von Kármán constant
		ν	Kinematic viscosity

*Corresponding Author. Tel: +91-11-26591179; fax: +91-11-26581119
E-mail address: pksen@am.iitd.ernet.in

#Current Address: Defence Institute of Advanced Technology, Pune – 411025, India

1. Introduction

The use of hydrodynamic stability theory to understand near wall turbulence was initiated by Malkus [1]. He conjectured that if the turbulent mean velocity profile is used in the Orr-Sommerfeld equation then it should be marginally stable. The results of Reynolds & Tiederman [2] showed quite conclusively the failure of Malkus's conjecture. Reynolds & Hussain [3-4] theoretically showed, using a three-way decomposition, that an extra term corresponding to the Reynolds stress appears in the governing equation for the disturbance. They used an isotropic eddy viscosity model for the Reynolds stress and obtained an extended Orr-Sommerfeld equation, however, they did not find any region of instability. Their experiments (Hussain & Reynolds, [5]) and theoretical results indicated that hydrodynamic stability theory may not be relevant to wall-turbulence. Sen & Veeravalli [6-7] considered the problem afresh and concluded that the inability of previous researchers to find any unstable modes was because of the selection of an isotropic eddy viscosity model, which is really not justified near the wall. Sen & Veeravalli [6-7] used a more realistic anisotropic eddy viscosity model (based on Pope, [8]) and found wall-mode instabilities. The solutions found by Sen & Veeravalli [6-7] mimicked some features of wall bounded turbulent flows like location of the production peak.

2. Sen & Veeravalli [7] Theoretical Formulation

Experimental results are based on Sen & Veeravalli [6-7], hence a brief outline of the theory is directly reproduced from Sen & Veeravalli [7] to provide the background in which the experimental results may be interpreted.

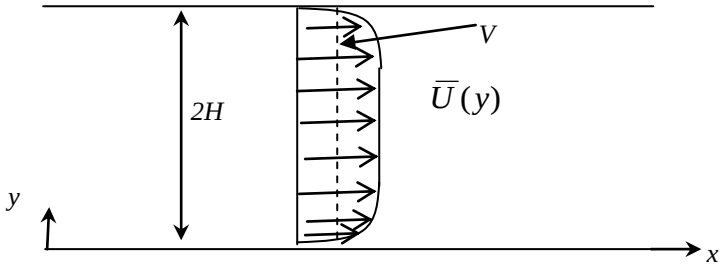

Fig.1. Turbulent channel flow

For the stability analysis the base flow is fully developed turbulent channel flow. In this an organised disturbance ($\tilde{u}$) is introduced. Thus Sen & Veeravalli (hereinafter denoted as S&V) [7] used a three way decomposition, similar to that of Reynolds & Hussain [3-4]

i.e. $$U_i = \overline{U}_i + \tilde{u}_i + u_i; \qquad P = \overline{P} + \tilde{p} + p \tag{1}$$

Where $\overline{U}_i, \overline{P}$ are respectively the time averaged velocity and pressure, $\tilde{u}_i$, $\tilde{p}$ are the contributions from the organised disturbance, and u_i, p are the respective turbulent fluctuations. Now by subtracting the time average of U_i from the ensemble (phase locked) average (denoted by $\langle\ \rangle$) the organised disturbance $\tilde{u}_i$ can be obtained. This procedure is true for pressure *P*.

i.e. $$\langle U_i \rangle - \overline{U}_i = \tilde{u}_i ; \langle P \rangle - \overline{P} = \tilde{p} \tag{2}$$

By applying this procedure to the incompressible Navier-Stokes and continuity equations we get

$$\frac{\partial \tilde{u}_i}{\partial t} + \overline{U}_j \frac{\partial \tilde{u}_i}{\partial x_j} + \tilde{u}_j \frac{\partial \overline{U}_i}{\partial x_j} = -\frac{1}{\rho}\frac{\partial \tilde{p}}{\partial x_i} + \nu \frac{\partial^2 \tilde{u}_i}{\partial x_j \partial x_j} + \frac{\partial \tilde{r}_{ij}}{\partial x_j} \tag{3}$$

$$\frac{\partial \tilde{u}_i}{\partial x_i} = 0$$

Where $$\tilde{r}_{ij} = -\left(\langle u_i u_j \rangle - \overline{u_i u_j}\right) \tag{4}$$

The disturbance was assumed to be very weak compared to background turbulence i.e.

$$\left|\langle \tilde{u}_i \tilde{u}_j \rangle\right| << \left|\langle u_i u_j \rangle\right| \tag{5}$$

S&V [7] modelled the time-averaged Reynolds stress tensor using anisotropic eddy viscosity model outlined in Pope [8]. Pope's model for time averaged Reynolds stress tensor is:

$$-\overline{u_i u_j} = -\frac{2}{3}k\delta_{ij} + \varepsilon\bar{s}_{ij} - \varepsilon C(k/\varepsilon_d)\left[\frac{1}{2}\left[\bar{\omega}_{ij}\bar{s}_{kj} - \bar{s}_{ik}\bar{\omega}_{kj}\right]\right] \tag{6}$$

Here, the eddy viscosity ε defined as $-\dfrac{\overline{u\upsilon}}{(d\overline{U}/dy)}$; k is the turbulent kinetic energy; ε_d is the dissipation rate of the turbulent kinetic energy and C is a constant. From the form of the above equation S&V [7] defined an anisotropy parameter λ as $C(k/\varepsilon_d)(d\overline{U}/dy)$. Thus the standard isotropic form of the eddy viscosity model is recovered when λ is zero. The ensemble averages of the Reynolds stress similarly is modelled as:

$$-\langle u_i u_j\rangle = -\frac{2}{3}k\delta_{ij} + \varepsilon\langle s_{ij}\rangle - \varepsilon(\lambda/\overline{U}')\left[\frac{1}{2}\left[\langle\omega_{ik}\rangle\langle s_{kj}\rangle - \langle s_{ik}\rangle\langle\omega_{kj}\rangle\right]\right] \tag{7}$$

The model for $\tilde{r}_{ij}$ is obtained by subtracting Eq. (6) from Eq. (7).

Now, in order to obtain the general solution to Eq. (3), they considered normal modes of the form,

$$\psi = \phi(y)\exp^{i\alpha(x-ct)} \tag{8}$$

As shown in S&V [7], Squires theorem is weakly valid and hence only the 2D problem was considered. With these above formulation they obtained the following extended Orr-Sommerfeld equation. As is clear from Eq. (8) $\phi(y)$ is the eigenfunction, α is the wave number and c is the wave speed.

$$\begin{aligned}
&i\alpha^+\left[\left(\overline{U}^+ - c^+\right)\left(\phi'' - \alpha^{+2}\phi\right) - \overline{U}^{+\prime\prime}\phi\right] - \left[\phi'''' - 2\alpha^{+2}\phi'' + \alpha^{+4}\phi\right] \\
&-\left[E^+\left\{\phi'''' - 2\alpha^{+2}\phi'' + \alpha^{+4}\phi\right\} + 2E^{+\prime}\left\{\phi''' - \alpha^{+2}\phi'\right\} + E^{+\prime\prime}\left\{\phi'' + \alpha^{+2}\phi\right\}\right] \\
&-\lambda^+E^+\left[-2i\alpha^+\phi''' + 2i\alpha^{+3}\phi'\right] - 2i\alpha^+\phi'\left[\lambda^+E^{+\prime\prime} + 2\lambda^{+\prime}E^{+\prime} + \lambda^{+\prime\prime}E^+\right] = 0
\end{aligned} \tag{9}$$

The superscript '+' indicates that all the variables have been normalised by the inner scales. In Eq. (9), the first group of terms in square brackets corresponds to the Rayleigh equation; the first two groups of terms in square brackets correspond to the classical Orr-Sommerfeld equation; and, the remaining terms constitute the modifications to the classical Orr-Sommerfeld equation based on anisotropy.

Sen & Veeravalli [6-7] solved the above Eq. (9) for the turbulent boundary layer as well as for channel flow. They were able to show the presence of unstable modes (T-S like wall modes with the inner peak in the buffer layer) in the near wall region for a wave number band. Figure 2 shows nearly identical behaviour for turbulent boundary layer as well as channel flow.

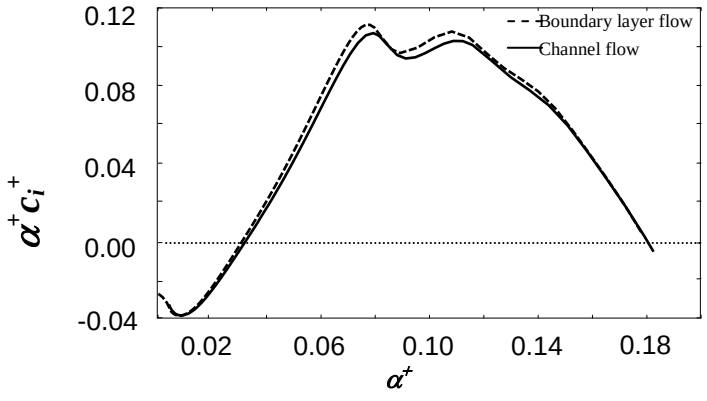

Fig.2. Growth rate curve from S&V [7], Reynolds Number is 5000 for both boundary layer and channel flow calculation.

3. Stability Experiments in a Turbulent Channel

Experiments were conducted to verify the results of S&V [7]. A 2-D channel was specially designed for this experiment.

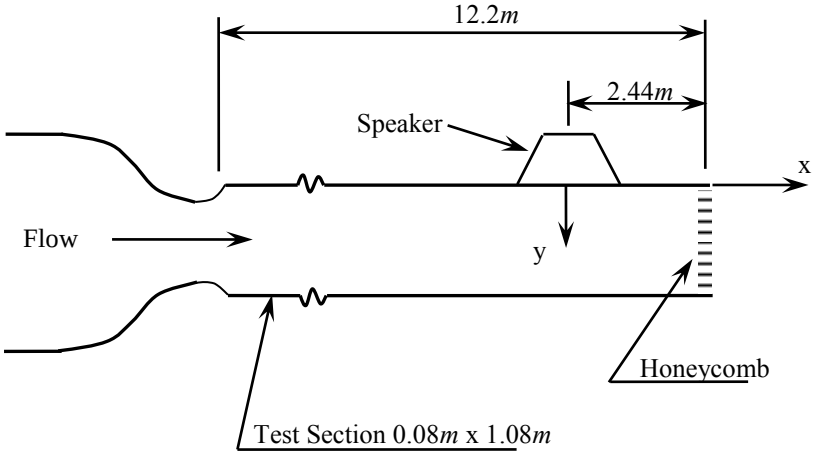

Fig.3. Schematic view of the set-up

Details about the experimental setup may be seen in Joshi [9]. Experiments were conducted for Re~14000. A hot-wire anemometer was used to obtain the turbulent data. The organised (sinusoidal) disturbance was generated by means of a speaker and was introduced through a span wise slot of size $1.5mm \times 100mm$ provided at the centre of the tunnel wall, $11.56m$ down stream of the entry to the channel. Different configurations were tried for introducing the organised disturbance. Three arrangements are shown in figure 4.

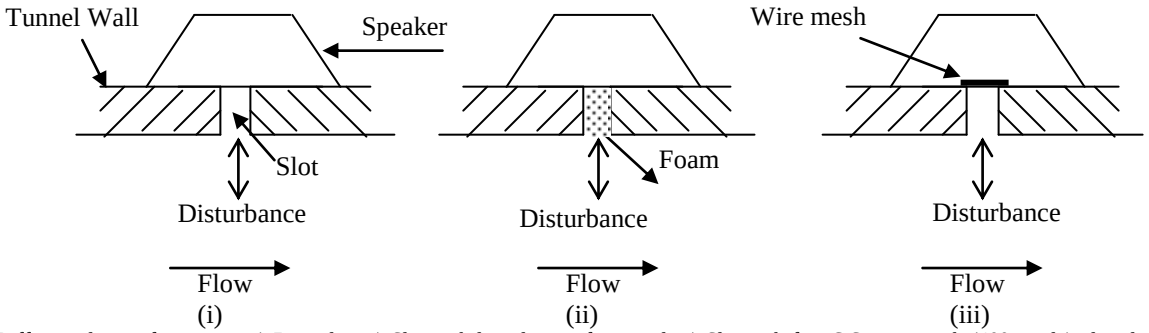

Fig.4. Different slot configurations. i) Bare slot; ii) Slot with low density foam and iii) Slot with fine S.S. wire mesh (400-grade) placed on the speaker side.

The configuration with the fine wire mesh (400-grade) was found to be the best setup for introducing the disturbance. A very detailed qualification was undertaken on the unperturbed and perturbed flow. Various checks were undertaken to ensure that the set-up and analysis procedures are adequate for resolving the organised disturbance and capturing its evolution. The detailed experimental results for all the above cases and qualification of the turbulent channel can be seen in Joshi [9].

The amplitude of the organised disturbance input to the speaker was set at 0.5V and the frequency was set to $300Hz$ for most of the experiments (the estimated wave number of this frequency is likely to lie close to the peak of the unstable range determined from S&V [7].

Repeatability of the eigenfunction was checked for organised disturbance of 300Hz, 0.5V and 7V. From figure 5a & 5b one can seen that degree of repeatability is remarkably good. In figure 5b results from an acoustic experiment (slot taped from out side, i.e. flow from the slot is blocked) shows the capability of the phase averaging method to extract even a very small disturbance due to vibration of the wall etc. As expected the amplitude of the eigenfunction for this case is very small (the peak value is approximately 20% of the amplitude of first two curves in figure 5b). The final curve in figure 5.b has been obtained with the speaker turned off. This result is an indicative of the error present in the phase-locked averaging process. As can be seen this error is quite negligible (less than 2.5% of the peak of the first curve). We are thus confident that our method of introducing the organised disturbance and extracting the eigenfunction through phase averaging is quite robust.

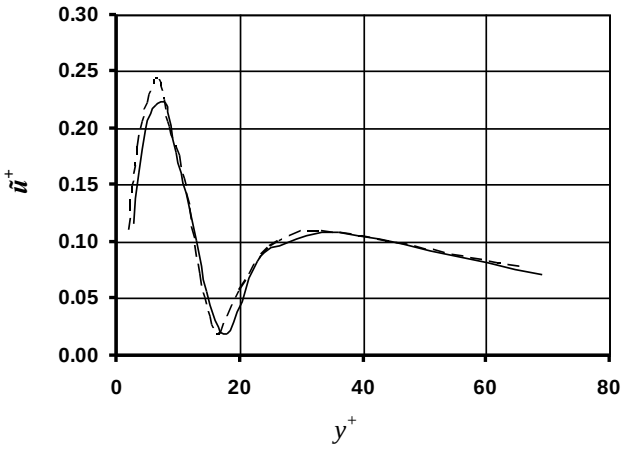

Fig.5a. Repeatability of the experiments. Dashed line and solid line shows the eigenfunctions measured on two different days with same hot-wire. Organised disturbance 300Hz 0.5V. Measurement station corresponds to $x = 10mm$.

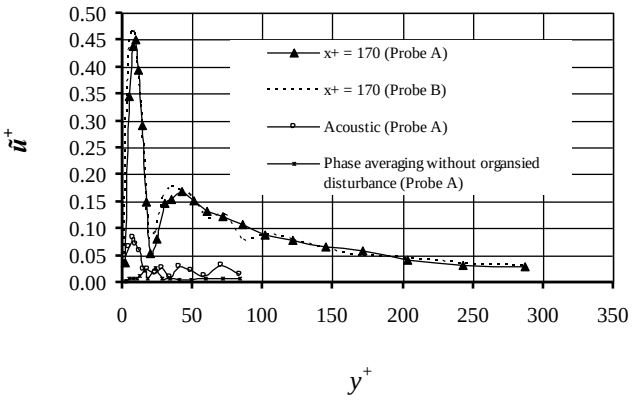

Fig.5b. Level of noise and acoustics on the eigenfunction. Organised disturbance 300Hz 7V Measurement station corresponds to $x = 10mm$.

4. Experimental Results & Discussion

Figure 6 shows a comparison between the calculated eigenfunction of S&V [7] with the experimentally obtained eigenfunction.

The non-dimensional wave number for the S&V [7] calculations has been set at $\alpha^+ = 0.057$, while, in the experiments it has been estimated to be approximately 0.058. Note that the vertical scale in the computations is arbitrary and it has been adjusted such that the magnitude of the inner peak of $\tilde{u}^+$ is the same as that in the experiments. We see that the eigenfunctions are qualitatively very similar. The location of the inner peak is slightly closer to the wall in the computations ($y^+ = 6.5$ as opposed to 8.0 in the experiments). Similarly the outer peak is also closer to the wall in the computations and its magnitude is lower. However, the location of the minimum in both cases is around $y^+ = 20$. The experimental eigenfunction extends much further into the body of the flow (beyond $y^+ = 300$). As discussed below this is probably due to several modes being excited by the speaker.

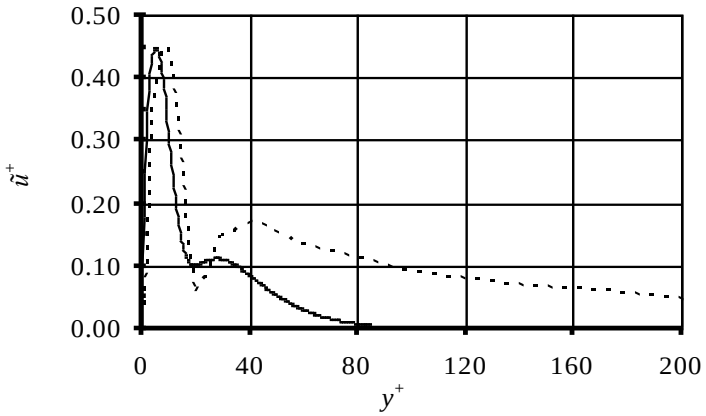

Fig.6. Comparison of our experimental eigenfunction (dotted line) with the theoretical results obtained by S&V [7], (solid line) at a Reynolds number of 5000, $\alpha^+ = 0.057$; $c_r^+ = 5.39$ and $c_i^+ = 1.05$.

Boundary excitation can generate different modes. Excitation can be from both sides, or can be from a single side. Hussain & Reynolds [5] used two sided excitation at low frequencies (25Hz to 100Hz) and obtained symmetric damped modes. In our present study, single sided excitation, at a higher frequency (as predicted by S&V [7]), resulted in unstable modes. Since the mode of interest is a wall mode, the outer boundary condition and the presence or absence of excitation in the other wall, should be irrelevant. It was not possible to modify our set-up to introduce two-sided excitation since the region of interest is

very close to the slot. However, in order to check the insensitivity of the measured eigenfunction to the outer boundary condition, we conducted experiments in a boundary layer of a wind tunnel (0.6m × 0.6m Test section). The organised disturbance was introduced through a speaker from the slot provided on the wall as in the case of the channel flow experiment. A comparison of the eigenfunctions obtained for the boundary-layer case and the channel case is shown in figure 7. The results show that the single side excitation is enough to get the TS-type wall mode. This is in agreement with the S&V [7] theory i.e., the eigenfunction for turbulent channel flow and boundary layer flow are similar.

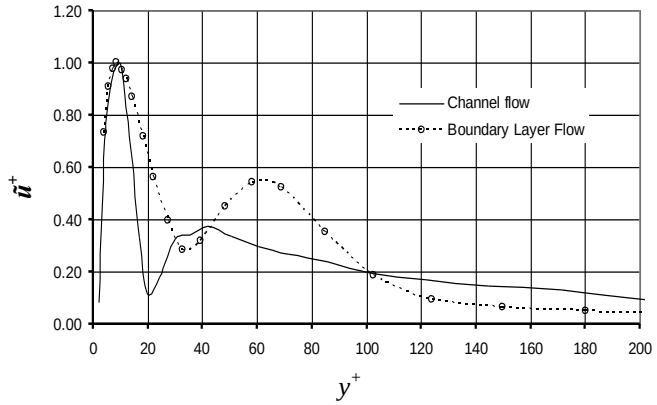

Fig.7. Eigenfunction for channel and boundary layer flow at a fixed disturbance frequency of 300Hz. Here the $\tilde{u}^+$ scaled arbitrarily to match the peak values. Measurement station corresponds to x = 10*mm*.

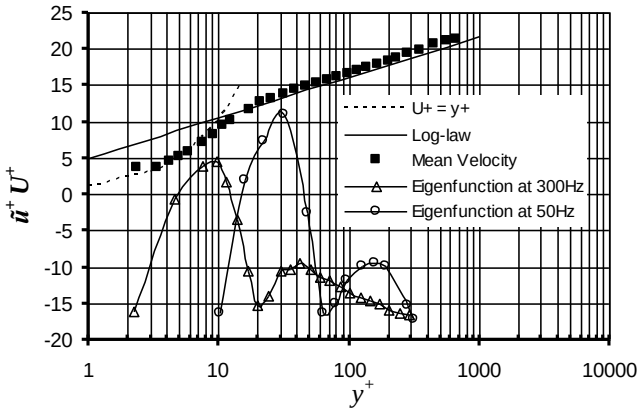

Fig.8. Mean velocity and Eigenfunction. Y- co-ordinate of the Eigenfunction is scaled such that it should appear with the mean velocity profile. Measurement station corresponds to x = 10*mm*.

Figure 8 shows a comparison between the modes obtained at 300Hz and 50Hz along with the mean velocity profile. It is clear that the wall mode (300Hz) has its primary peak in the buffer region, while the other mode (50Hz) which belongs to a class studied by Hussain & Reynolds [5], has its peak in the log region and where one will get only decay. Hence the modes studied by Hussain & Reynolds [5] are really not relevant to our work.

Another question is whether or not we can compare experimental (spatial) results with theoretical (temporal) results. So long as linear near-neutral disturbances are considered, spatial and temporal growth rates are related through the group velocity, c_g , as shown by Gaster [10]. In our problem we focus on mildly amplified near wall, boundary-layer like modes.

This being so, no appreciable difference is expected between spatial and temporal eigenfunctions. A comparison of $\tilde{u}_{rms}$ profiles obtained from theory for both temporal and spatial cases is shown in figures 9 below. To permit easy comparison, the $\tilde{u}_{rms}$ curves have been normalized by the maximum values of $\tilde{u}_{rms}$. The two curves are virtually identical.

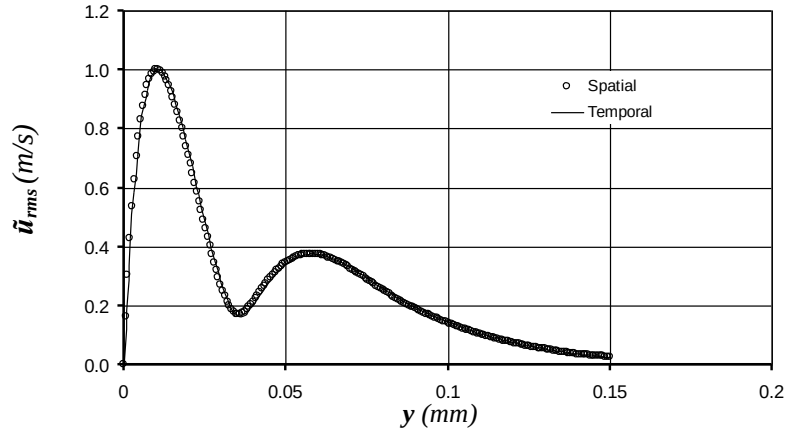

Fig.9. Graph of $\tilde{u}_{rms}$ versus y. For temporal case: α = 49, Re = 5000, c_r =0.35162439 and c_i =0.00601114. For spatial case: β = 17.2284, Re = 5000, α_r =49.3012 and α_i =-0.8135.

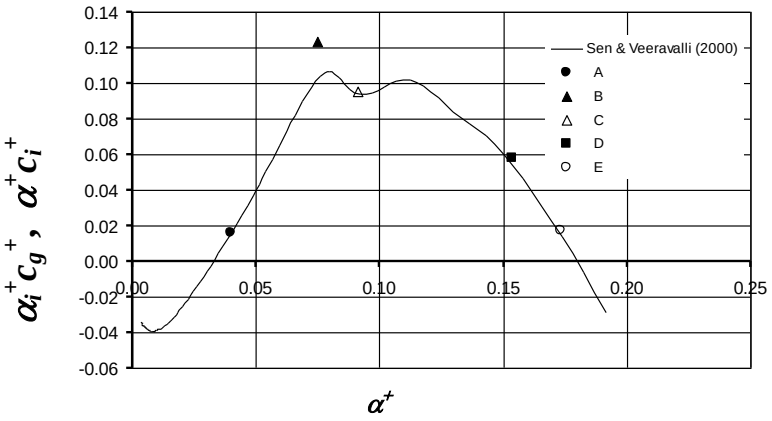

Fig.10. Growth rate curve $\alpha_r^+ c_i^+$ versus α_r^+ (inner variable scaling). Solid line is the temporal growth curve from S&V [7]. Symbols indicate the equivalent growth rate obtained for the 5 spatial cases studied (A to E). Reynolds Number is 5000.

Further we have chosen five different disturbance frequencies for comparing the growth rate obtained for the spatial and temporal calculations. The frequency values (labelled A, B, C, D and E) have been chosen such that they span the entire unstable range of the growth rate curve computed by S&V [7]. Except for one isolated case (near the most unstable region) the match is very good. Each from figure 9 and 10 it is clear that we can compare temporal growth rates from S&V [7] with our spatial growth rates from experiments over nearly the entire unstable band in α .

Evolution of eigenfunction was observed 3*mm* from the slot centre to about 12*mm* down stream. Figure 11a below shows measurements very close to the source of the disturbance (3*mm* to 8*mm*). At 3*mm* and 5*mm* it appears that there is competition between three modes, (i) the mode of interest which is a wall mode, (ii) another wall mode; and (iii) an outer mode. The second wall mode (ii) dominates at x = 3*mm*, decays rapidly, and effectively disappears by x = 8*mm*. The outer mode decays more slowly and is still visible in the profile at x = 8*mm*. The wall mode, of interest to us (i) is clearly discernible at x = 8*mm*. Note, x = 8*mm* corresponds to x^+ = 132 (1*mm* = 16.5 wall units). The normalised wave length, λ^+, of the organised disturbance (300Hz) is about 108. In our experiments, for all disturbance frequencies, we observed that the proper eigenfunction is obtained approximately 1.25 times the wavelength of the organised disturbance downstream of the slot. Klingmann et al. [11] observed a similar behaviour for TS waves in laminar boundary layer flow. Also the TS-like mode should show a π jump in the phase plot at the minimum of the eigenfunction.

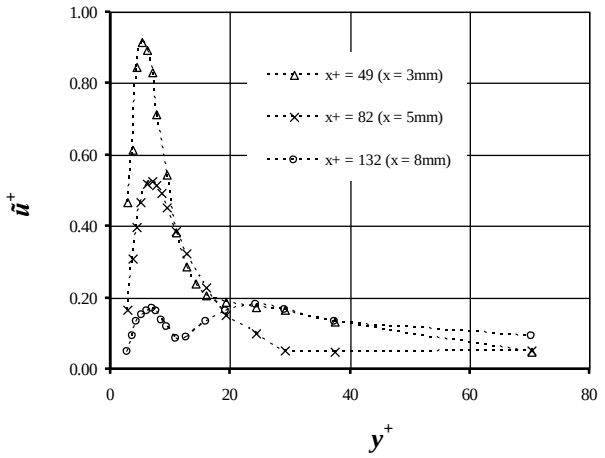

Fig.11a. Evolution of eigenfunction very close to the slot.

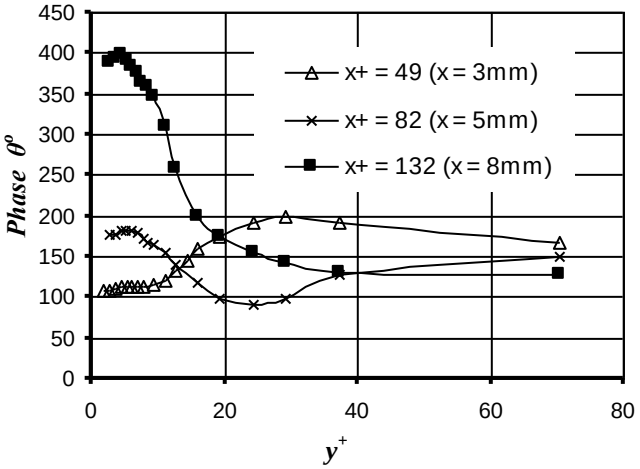

Fig.11b. Evolution of phase lag (θ)

One can see from figure 11b that there is no π jump at 3*mm* and 5*mm* but at 8*mm* there is a π jump. That means the required eigenfunction starts forming after 8*mm*. If we measure in the further downstream direction i.e. (8*mm* to 10*mm*) each of the curves in the figure 11c shows the presence of two peaks. In the first four stations the inner peak shows rapid growth, while, between the fourth and fifth stations the value of the inner peak remains unchanged. Each eigenfunction has a π jump at the minimum of the eigenfunction, as seen in figure 11d.

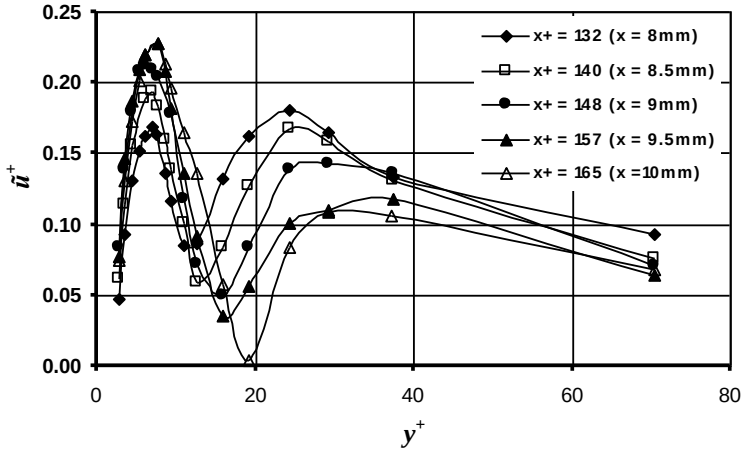

Fig.11c. Evolution of the eigenfunction in the vicinity of the slot.

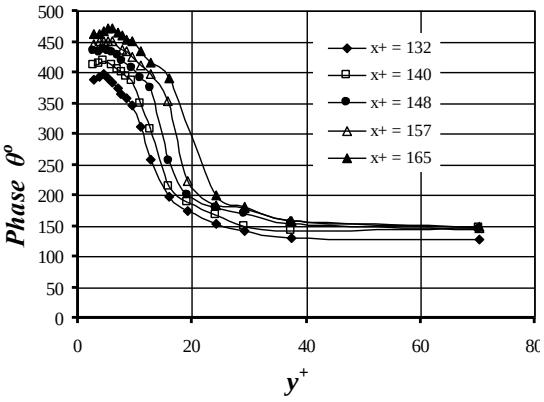

Fig.11d. Evolution of phase lag (θ)

Beyond $x = 10mm$ the inner peak also decreases and the location of the inner peak moves progressively away from the wall as shown in figure 11e.

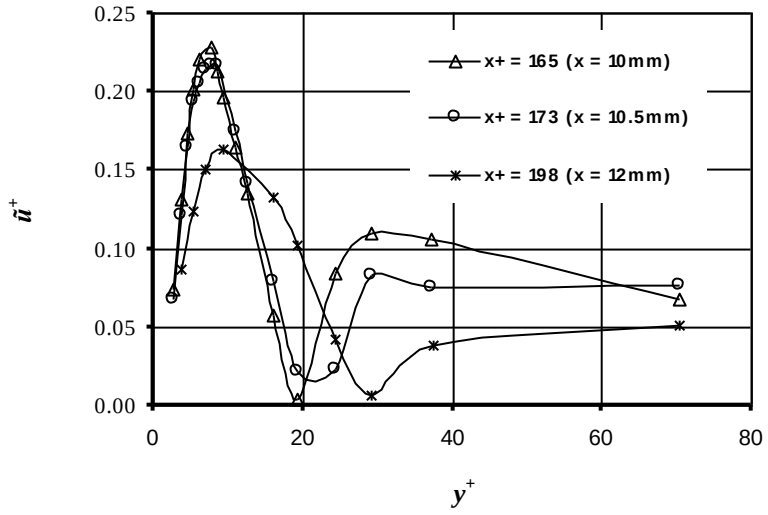

Fig.11e. Evolution of eigenfunction larger downstream distances.

In figure 12 the theoretical growth rate is shown as a function of the wave number. In this figure the points indicate the data obtained from the present experiments. Growth rates were calculated for different disturbance frequencies from 200*Hz* to 600*Hz* with amplitude of 0.5V. We see that the match between the experiments and the theoretical curve is quite good especially in the region where the curve is rising. Experiments at higher (>600Hz) frequencies indicate that the eigenfunction peaks shift towards the slot. Once the error bars are included, we see that the experimental growth rates are fully consistent with the theoretical curve obtained from S&V [7]. At lower frequencies (≤200Hz) the eigenfunction decay continuously and the growth rate is negative. On the other hand if we use the decay region (far down stream) of the data taken at 300*Hz* and calculate an effective growth rate (point 12 in figure 12) it does not lie anywhere near the theoretical curve. The linear theory presented in S&V [7] cannot explain a period of growth followed by decay.

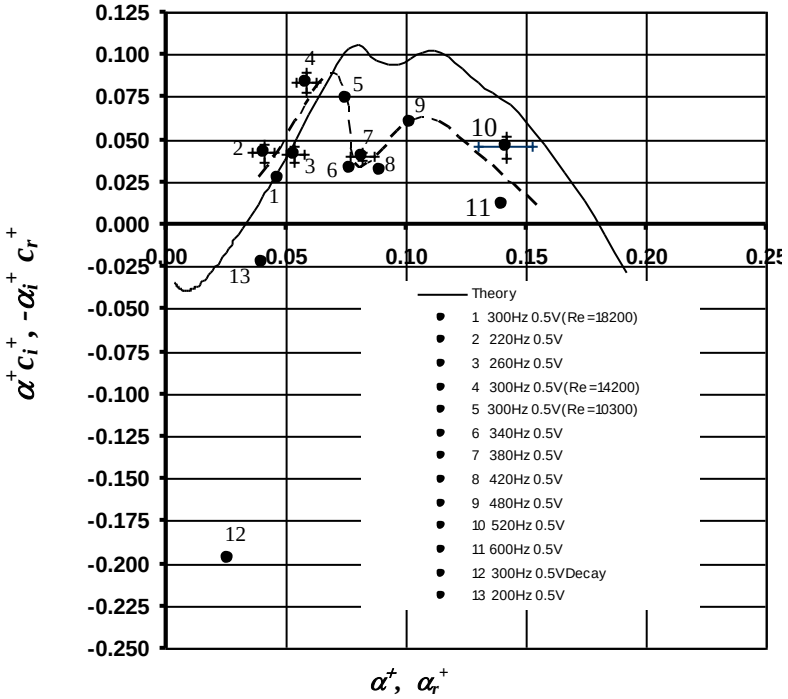

Fig.12. Growth rate curve $\alpha_r^+ c_i^+$ versus α_r^+ (inner variable scaling), Reynolds Number for the theoretical curve (solid line) is 5000. The curve is from S&V [7]. The points are from present experiments. The dotted line shows a rough trend passing through the experimental points. Unless explicitly mentioned the Reynolds number for the experiments is 14,000.

Figure 13 shows the evolution of the inner peak of the eigenfunction for different cases. The data at 300Hz show a clear region of growth followed by decay, while the data at 50Hz show uniform decay. One point of departure from S&V [7] is the decay observed in the experiments after an initial period of growth. Different ideas to explain the decay process were examined. Some candidates are; transient growth of non-normal modes, energy transfer between the organised disturbance and the corresponding disorganised disturbance (see chapter 5, Joshi [9]) etc. However the only possible explanation seems to be the break down of the two dimensionality of the instantaneous wave due to differential growth rates at different spanwise locations due to the presence of Klebanoff modes (K – modes). These are very similar to streaks in wall turbulence. A similar phenomenon was observed by Fasel [12] in his DNS work on a Klebanoff modes.

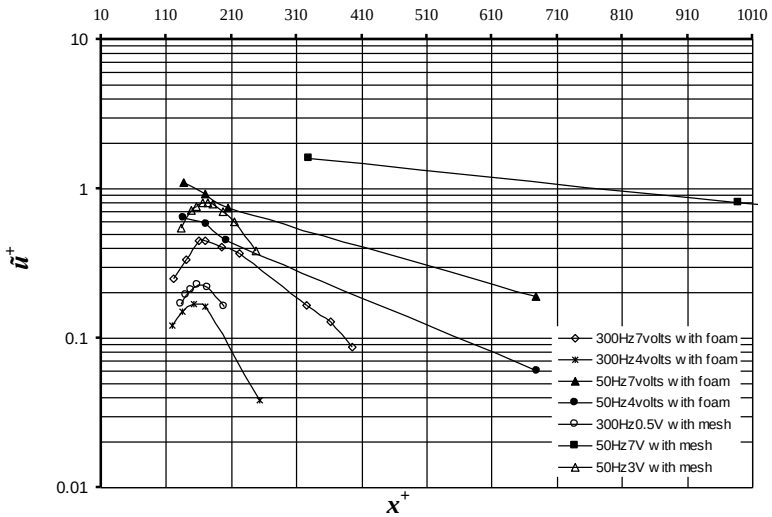

Fig.13. Evolution of inner peak of the eigenfunctions.

5. Conclusions

Our experimental results confirms the existence of TS – type modes in near wall turbulent flows and show fairly strong evidence in support of the theory outlined in S&V [6-7]. The eigenfunctions obtained in turbulent channel and boundary layer experiments are nearly identical, in the vicinity of the inner peak. This is consistent with the theoretical results of Sen and Veeravalli which show that the modes of interest are independent of outer boundary conditions. The shapes of the calculated and measured eigenfunctions are in good agreement. In the region of growth of the inner maximum the experimentally observed parameters (wave number, wave speed, growth rate and other parameters) are in good agreement with the theoretical results. Thus the claim made in S&V [6-7] that linear stability theory provides vital clues to understanding the mechanism of sustenance of turbulence in wall-bounded flows, has been corroborated.

Sen et al. [13] have shown that the interaction of 2D TS, 3D TS and Klebanoff modes can lead to explosive growth similar to the bursting phenomenon in wall turbulence. The 2D TS wave is a vital component of this mixture. Further Josan [14] and Sen et al. [15-16] have shown that the entire band of 2D TS waves could be suppressed by using compliant walls. This has serious implications for control of wall turbulence.

Acknowledgements

The support of the staff of the Gas Dynamics Laboratory (Dept. of Applied Mechanics, IIT Delhi), in particular Mr. R. P. Bhogal, is gratefully acknowledged.
An earlier version of this work was presented by Veeravalli et al. [17].

References

[1] Malkus W. V. R., 1956. Outline of a theory of turbulent shear flow, J. Fluid Mech., 1,521-539.
[2] Reynolds W. C., and Tiderman W. G., 1967. Stability of turbulent channel flow, with application to Malkus's theory, J. Fluid Mech., 27, 2, 253-272.
[3] Hussain A.K.M.F. and Reynolds W.C., 1970. The mechanics of an organized wave in turbulent shear flow, J. Fluid Mech., 41, 2, 241-258.
[4] Reynolds W.C. and Hussain A.K.M.F., 1972. The mechanics of an organized wave in turbulent shear flow Part 3. Theoretical models and comparison with experiments, J. Fluid Mech., 54, 2, 263-288.
[5] Hussain A.K.M.F. and Reynolds W.C., 1972. The mechanics of an organized wave in turbulent shear flow Part 2. Experimental results, J. Fluid Mech., 54, 2, 241-261.
[6] Sen P.K. and Veeravalli S.V., 1998. On the behaviour of organized disturbances in a turbulent boundary layer, Sadhana, 23, 167-193.
[7] Sen P.K. and Veeravalli S.V., 2000. Behaviour of organized disturbances in fully developed turbulent channel flow, Sadhana, 25, 423-437.
[8] Pope S. B., 1975. A more general effective-viscosity hypothesis, J. Fluid Mech., 72, 2, 331-340.
[9] Joshi, G.N., 2011. Experimental investigations on the relevance of hydrodynamic stability theory to wall-turbulence, PhD thesis, IIT Delhi.
[10] Gaster M., 1962, A note on the relation between temporally-increasing and spatially-increasing disturbances in hydrodynamic stability, J. Fluid Mech., 14, 02, 222-224.
[11] Klingmann B. G. B., Boiko A. V., Westin K. J. A., Kozlov V. V. and Alfredsson P. H., 1993, Experiments on the stability of Tollmien-Schlichting waves, J. Fluid Mech., 12, 4, 493-514.
[12] Fasel H. F., 2002, Numerical investigation of the interaction of the Klebanoff-mode with a Tollmien-Schlichting wave, *J. Fluid Mech.*, 450, 1-33.
[13] Sen P.K., Veeravalli S. V., Carpenter P. W., Joshi G. and Josan P. S., 2007, Organised structures in wall turbulence as deduced from stability theory-based method, *Sadhana*, Vol. 32, Part 1 & 2, 51-64.
[14] Josan P. S., 2004, Suppression of wall turbulence using a compliant surface based on stability and turbulence analysis, *Ph.D. Thesis*, I.I.T. Delhi, New Delhi.
[15] Sen P.K., Josan P.S.,Veeravalli S. V., and Carpenter P. W., 2006, Suppression of wall turbulence by stability turbulence analysis using a compliant surface., Proc Indian Natn Sci Acad, 72, 3, 159-166. (http://www.insa.ac.in)
[16] Sen P.K., Josan P.S. and Veeravalli S. V., 2006, Suppression of wall turbulence based on stability and turbulence analysis using a compliant surface. 6th *IUTAM symposium on Laminar-Turbulent Transition*, Editor: R Govindarajan, Springer, 231-236.
[17] Veeravalli S V, Sen P K & Joshi G, Stability theory and turbulent wall flow, Proc. *37th National & 4th International conference on FMFP*, FMFP10 – KN -11, 1-10, December 16-18, 2010, IIT Madras, Chennai, India.